This is a previous version of the article published in Materials Research Bulletin. 2017, 93: 102-111. doi:10.1016/j.materresbull.2017.04.040

Pd and Cu-Pd nanoparticles supported on multiwall carbon nanotubes for H_2 detection

Pascual Navarro-Botella, Jaime García-Aguilar, Ángel Berenguer-Murcia[*], *Diego Cazorla-Amorós*

Inorganic Chemistry Department and Materials Science Institute, Alicante University, Ap. 99, E-03080, Alicante, Spain

Abstract

Pd, Cu and bimetallic Cu-Pd (denoted as Cu_xPd_{1-x} where *x* indicates the Cu molar ratio) nanoparticles protected by polyvinylpyrrolidone (PVP) have been synthesized by the reduction-by-solvent method (modified by the addition of $NaBH_4$ in the case of Cu-based nanoparticles) and deposited by a very simple method on multiwall carbon nanotubes (MWCNTs). The resulting materials were tested as H_2 sensors at room temperature under ambient pressure conditions. The effect of the total metal loading and the nanoparticles composition have been analysed in H_2 detection tests in synthetic air (3.3 % vol.). H_2 concentration was varied from 0.2 to 3.3 % vol. in order to assess the sensitivity of the prepared devices, and N_2 was also used as carrier gas to evaluate the sensing performances (recovery and response time) and the main detection mechanism in this kind of materials. In this sense, these sensors have shown a very low response time for all the H_2 concentration range, so this simple preparation procedure results cost-effective and highly efficient H_2 sensors that may perform very well under real application conditions and even in oxygen-depleted atmospheres.

[*]Corresponding author. Fax: +34 965 903454
E-mail: a.berenguer@ua.es (Á. Berenguer-Murcia)

INTRODUCTION

Nowadays hydrogen is considered as a key element to develop the new sustainable energy model. The present energy perspectives focus on the production of H_2 by the electrolysis of water through renewable energy sources and the reforming of hydrocarbons such as ethanol or other organic compounds (Abbasi and Abbasi, 2011) to be further stored and used in fuel cells. H_2 is a colourless and odourless gas, with high diffusivity, highly flammable at concentrations above 4% vol., and explosive over a wide range of concentrations (15-59 %) at standard atmospheric pressure (Boon-Brett et al., 2010). Therefore, safety issues concerning its generation, transport, storage and use must always be considered. For this purpose, the availability of hydrogen sensors is mandatory. Concerning hydrogen sensors, there is a wide variety of systems capable of measuring different kinds of signals usually based on materials such as optical fibers or semiconductors (Hübert et al., 2011). Continuous efforts are being made in order to improve sensitivity, selectivity, response time and reliability, as well as diminishing production costs, size and power consumption of the devices, to meet the demands of a future H_2 economy scenario (Boon-Brett et al., 2010).

Carbon-based materials have been used in many different fields such as catalysis, adsorption, energy storage and thermal/electric conductivity applications (Inagaki et al., 2014). Due to their extraordinary properties novel carbon nanomaterials, such as, carbon nanotubes (CNTs), carbon nanofibers (CNFs) or graphene, are some of the emerging materials in these kind of applications (Du et al., 2014; Shenderova et al., 2002). Carbon nanomaterials have been also studied in sensing applications of H_2 and other gases (NH_3, NO_2…). In the literature, the most widely studied carbon material for this application has been CNTs, be it either Single-Walled (SWCNTs) or Multi-Walled (MWCNTs) (Goldoni

et al., 2010). Some works may also be found with SnO_2-CNFs based devices for H_2 sensing (Wang et al., 2015).

To increase the interaction between CNTs and H_2 at ambient conditions (room temperature and pressure) the addition of some noble metal, as Pd or Pt becomes mandatory. This noble metal acts as intermediate between the adsorbed/absorbed H_2 analyte and the carbon material (Kumar and Ramaprabhu, 2006). Many methodologies have been used to deposit the detection active phase over the carbon material support in the case of noble-metal based devices. Sputtering, electron beam evaporation or synthesis using dendrimers to link the metal nanoparticles to CNTs are examples found in the literature (Ju et al., 2010; Randeniya et al., 2012) and in all cases more complicated compared to the independent synthesis of metal nanoparticles (by the polyol reduction method) and the posterior deposition on the carbon material with a micropipette (García-Aguilar et al., 2014a). In this sense, the use of transition metals alloys with Pd or Pt is a great means to diminish the noble metal loading and thus the final cost of the device; Ni has been used as NiPd alloy for the same application (García-Aguilar et al., 2014a; Lin and Huang, 2012; Phan and Chung, 2014).

In this study we report the preparation of H_2 sensors at room temperature based on Pd, Cu and Cu_xPd_{1-x} nanoparticles loaded over a carbon nanomaterial by a very simple, low-cost procedure, using MWCNTs as support. The methodology used to synthesize the nanoparticles was the well-established reduction by solvent method (modified by the addition of $NaBH_4$ in the case of Cu nanoparticles). The prepared nanoparticles were deposited with a micropipette over a MWCNT layer previously laid down on the selected substrate (from a dispersion in DMF). The influence of the nanoparticle loading in the devices, and the Pd ratio in the nanoparticles was studied in standard H_2 detection tests (3.3 % vol.) using synthetic air as carrier gas. In order to evaluate the response and

recovery time and the detection mechanism of these devices the effect of H_2 concentration in the inlet stream as well as performing the detection experiments in an oxygen-free atmosphere were also carried out.

MATERIALS AND METHODS

MWCNTS SUSPENSIONS

MWCNTs (bamboo-type MWCNT and with a diameter between 15-30 nm) were used as supports in this study. Suspensions of MWCNTs with different concentrations were prepared using DMF as solvent (N, N-dimethylformamide, 99.9 %, Sigma-Aldrich). In a representative example, 200 mg of MWCNTs were dispersed in 10 ml of DMF (20 mg/ml) and sonicated for 10 min in an ultrasound probe (Bandelin Sonoplus GM2200, 200 W) at 25% output power.

SYNTHESIS AND PURIFICATION OF THE METAL NANOPARTICLES

Pd metallic nanoparticles were synthetized following the reduction-by-solvent method as we have reported previously (García-Aguilar et al., 2014b; Miguel-García et al., 2015). The palladium precursor (Pd acetate, 98 %, Sigma Aldrich) was dissolved in 25 ml of 1,4-dioxane, and the capping agent (PVP 40T, Sigma Aldrich) was dissolved separately in 60 ml of ethylene glycol at 80ºC under magnetic stirring. In this synthesis 0.5 mmol of metal were used in total and the PVP (taken as monomer)/Metal molar ratio was set to 10. After complete dissolution of the solids, the PVP solution was cooled down to 0 ºC and the Pd precursor solution was injected under vigorous stirring. A 1M NaOH solution was added dropwise in order to adjust the pH to 9. Then, the final solution was heated at 100ºC under vigorous magnetic stirring. Formation of the metallic nanoparticles was evidenced when

the solution changed its colour from yellow to dark brown. The entire process is carried out under Argon atmosphere by means of a Schlenk system. When the nanoparticles are synthesized it is necessary to perform a purification stage in order to remove the excess surfactant as well as all the reagents used during the synthesis. The prepared colloids were then purified in an excess of acetone and redispersed in the appropriate amount of methanol, so that the final metallic concentration in this solvent is perfectly known (Domínguez-Domínguez et al., 2006). The nanoparticles suspension obtained by this procedure is stable against agglomeration for a long period of time.

In the case of pure Cu and Cu_xPd_{1-x} nanoparticles, due to the significantly lower reduction potential compared to Palladium, the same procedure as described above did not result in all the Cu being reduced. This was evidenced during the purification step, in which the acetone phase (supernatant liquid) showed a blue colour typical of Cu(II). For this reason, we decided to modify the reduction protocol of the Cu-based mono- and bimetallic nanoparticles by the addition of $NaBH_4$ during the synthesis. It must be noted that even following this synthetic procedure the purification of pure copper nanoparticles resulted in the same blue colour in the supernatant phase, indicative of the presence of Cu(II) species, thus evidencing that the procedure had not been successful. Basing ourselves in previous reports in which a similar procedure for nanoparticles synthesis was conducted directly on carbon supports (Zaragoza-Martín et al., 2007) we decided to introduce the MWCNTs in the nanoparticles solution synthesis, resulting in the following synthesis protocol for Cu and Cu_xPd_{1-x} nanoparticles with the MWCNTs: The Cu precursor ($Cu(NO_3)_2 \cdot H_2O$, 99.999 %, Sigma-Aldrich) and the necessary amount of commercial MWCNTs were mixed with the PVP dissolved in absolute ethanol. This mixture was heated at 50ºC for 2 h. The necessary amount of Pd precursor was added, maintaining the temperature at 50ºC. Before the pH adjustment by addition of aqueous NaOH the solution was cooled at 0ºC in

an ice-bath, and 0.010 g of $NaBH_4$ (Sigma-Aldrich) were added to the mixed solution to produce the reduction of both metals. The solution was then stirred for 12 hours. Then, the resulting metal loaded MWCNTs were filtered and washed to remove the excess of reactants. Finally, the MWCNTs with the Cu and Cu_xPd_{1-x} nanoparticles were redispersed in DMF using the same aforementioned procedure.

DEVICES PREPARATION

Glass slides (24 x 24 mm, Menzel-Gläser), previously washed with ethanol, were used as supports for the devices. Two adhesive copper strips (Copper Conductive Tape, EMS) were set with a separation of approximately 6 mm to serve as connections for the multimeter (6 ½ Digit Multimeter, Agilent). A small layer of silver-epoxy paint (Two-Part Epoxy Adhesive Conductive Silver, EMS) is applied between the interface of the copper strips and the glass slide to improve the electrical contact. After the silver-epoxy paint was already dried and cured, 160 μl of the freshly sonicated MWCNTs were added between the two copper connections by means of a micropipette to close the electrical circuit. The resulting systems were dried at room temperature overnight. Finally, in the case Pd-based devices, the necessary amount of Pd suspension was added and dried also at room temperature, as reported previously (García-Aguilar et al., 2014a). Figure 1 shows a representative scheme of the preparation of Pd/MWCNTs-based devices as well as an image of a sensing device.

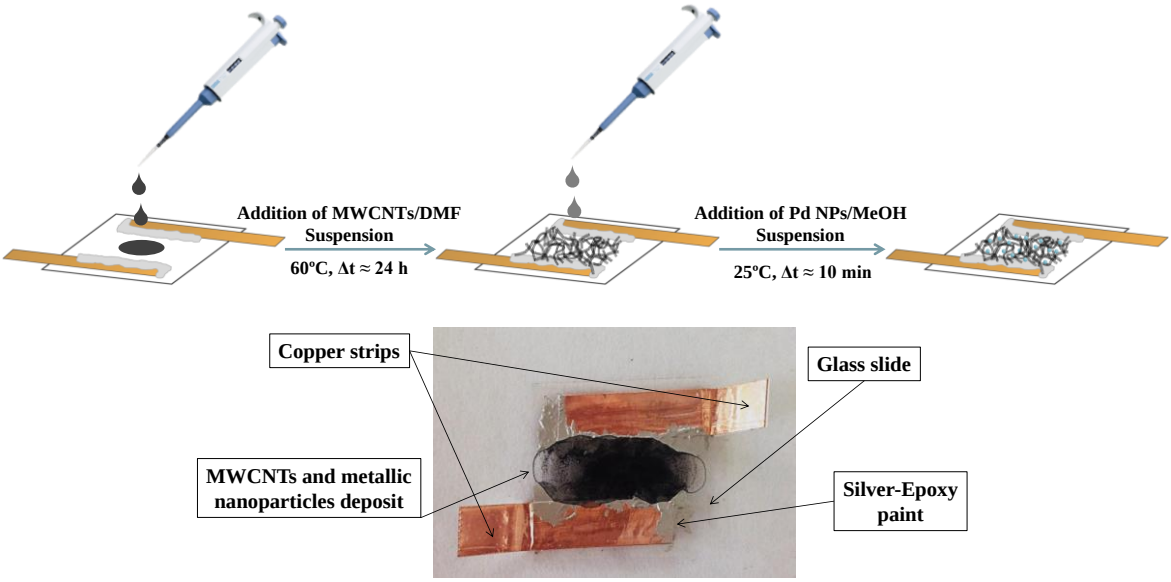

Figure 1| Top: Scheme of the Pd/MWCNTs-based device preparation for H_2 detection at room temperature; Bottom: Image of the assembled device detailing all its components.

Table 1 shows a summary of the samples prepared in this work, studying the Pd metal loading over the MWCNTs deposit and the different CuPd ratios used.

Table 1. Summary of the samples prepared and tested in H_2 detection tests.

Sample	Metal	Metal Loading (wt%)[a]
0.3-Pd	Pd	0.3
0.6-Pd	Pd	0.6
1.2-Pd	Pd	1.2
2.5-Pd	Pd	2.5
1.2-$Cu_{0.25}Pd_{0.75}$	$Cu_{0.25}Pd_{0.75}$	1.2
1.2-$Cu_{0.5}Pd_{0.5}$	$Cu_{0.5}Pd_{0.5}$	1.2
1.2-$Cu_{0.75}Pd_{0.25}$	$Cu_{0.75}Pd_{0.25}$	1.2
1.2-Cu	Cu	1.2

[a] *The nominal metal loading has been calculated from the amount of metal deposited and the MWCNTs weight.*

SAMPLES CHARACTERIZATION

The metal nanoparticles composition in the samples was measured by X-ray Photoelectron Spectroscopy (XPS) using a K-Alpha instrument (Thermo-Scientific), equipped with an Al anode. For the analysis, the MWCNTs were first deposited on the sample holder and then the metal nanoparticles were loaded on them. Characterization of the electronic states of each element was made from the relative area of the peak corresponding to each electronic state after deconvolution of the XPS signal. Binding energies are referenced to the C1s peak assumed to have a binding energy of 284.5 eV. The metal composition of the Cu and Pd in the bimetallic nanoparticles was analyzed by inductively coupled plasma-optical emission spectroscopy (ICP-OES), in a Perkin-Elmer Optima 4300 system. The extraction of the metal was made by treating the samples with aqua regia at room temperature and diluting the samples to a final concentration between 10-20 ppm. The morphology of the

sensors was studied by Scanning Electron Microscopy (SEM) using a JEOL JSM-840 equipment. The samples were also characterized by Transmission Electron Microscopy with the instrument (JEOL JEM-2010) operating at 200 kV with a space resolution of 0.24 nm. For the analysis, a small amount of the sample was suspended in a few drops of hexane, and sonicated for a few minutes. A drop of this suspension was then deposited onto a 300 mesh Lacey copper grid and left to dry at room temperature. TEM analyses allowed the determination of the metal particle size.

H_2 DETECTION TESTS

H_2 sensing tests were carried out in a custom-built gas cell connected with stainless steel tubing (1/8" o.d.) to the gas lines used in the analyses. For the measurements, the sensors were placed inside a Teflon cell, which was then sealed with a polycarbonate lid and fitted with a Viton O-ring to prevent leaks. A constant gas flow was passed through the cell by means of mass flow controllers (Bronkhorst), while the resistance of the samples was monitored simultaneously with a multimeter (6 ½ Digit Multimeter, Agilent).

The experiments were performed at ambient conditions (room temperature and pressure) with a constant gas flow of 90 ml/min. In standard H_2 sensing experiments, synthetic air is used as carrier gas until a constant resistance value of the device is reached. Then, the gas flow is switched to a mixture containing 3.3 % vol. H_2 in air for 4 minutes, enough time to observe a resistance change. Finally, the stream was switched back to synthetic air for 10 minutes in order to completely purge the cell and recover the initial resistance value. Experiments were also performed at different H_2 concentrations (using synthetic air as carrier gas) in order to evaluate the sensitivity of the sensor. In order to obtain reproducible and reliable resistance measurements, a conditioning step of the sensors

consisting of three consecutive H_2/air switches was carried out. All the results shown in this work correspond to samples that were submitted to this preliminary conditioning step unless stated otherwise.

Another set of tests were carried out using N_2 as carrier gas in order to determine the hydrogen detection mechanism in this kind of devices, as it has been reported previously for similar devices (García-Aguilar et al., 2014a; Randeniya et al., 2012).

The sensitivity of the sensor (ΔR_H) was calculated according to the following equation:

$$\left|\Delta R_H\right| = \frac{\left|R_H - R_O\right|}{R_O} \times 100$$

where R_H is the resistance of the sample at a given time and R_O is the initial resistance before each H_2 switch.

Two crucial parameters were evaluated for the different materials presented in this study, namely the response time and recovery time (Boon-Brett et al., 2010). The response time as presented in this study has been defined by previous authors as the time needed for the sensor to reach a relative resistance value of 36.8 % of the maximum signal measured under the described experimental conditions (Ju et al., 2010). Furthermore, the recovery time as analyzed in our work has been defined as the time that the sensor needs for the measured signal to reach the R*o* value after the H_2 switch (Randeniya et al., 2012). It should be mentioned, for the sake of clarity towards critical comparison of the results, that other authors (Kaniyoor and Ramaprabhu, 2011) define the response time of the sensor as the time taken for the resistance to change from its initial value to 90% of the highest measured value, while the recovery time is defined as the time taken for the resistance to decrease to 10% of the highest measured value.

RESULTS

Pd, Cu AND Cu_xPd_{1-x}/MWCNT CHARACTERIZATION

The prepared MWCNT deposits were analysed by electron microscopy (TEM and SEM) to determine the morphology of the carbon material prepared using the DMF suspension (20 mg/ml) in this work. In Figure 2, some representative micrographs are presented for both SEM and TEM analysis of the MWCNTs deposited on the glass slide.

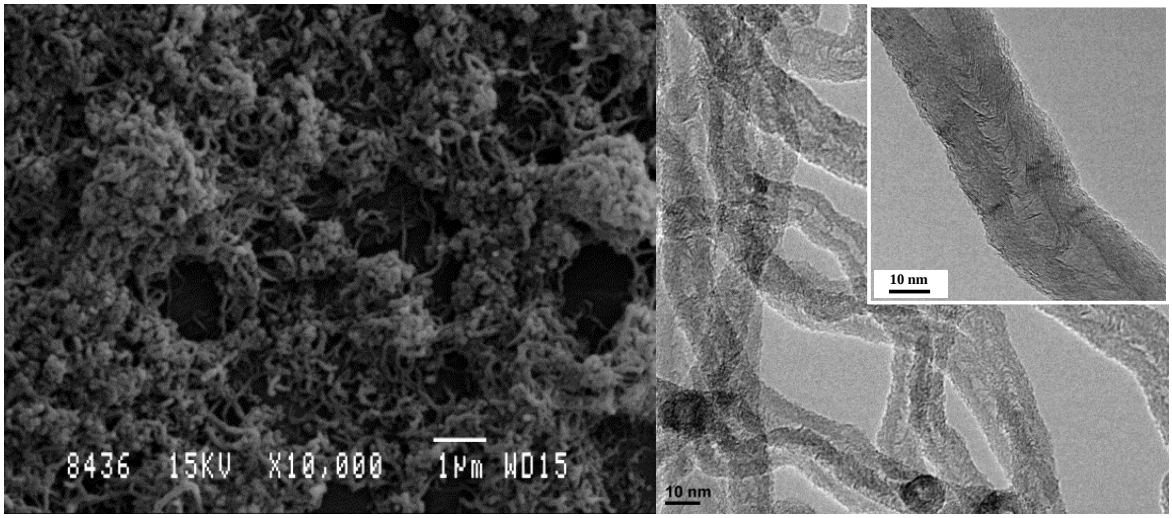

Figure 2| SEM image of MWCNTs/DMF deposit on the glass slide in the device (left) and TEM pictures of individual MWCNTs (right).

In Figure 2 (left) it is possible to observe that the MWCNTs are bundled to a large degree. This entanglement is most likely produced during the evaporation of the DMF. This kind of deposit is also observed with SWCNT using the same solvent and its occurrence is attributed to the absence of any surfactant species (García-Aguilar et al., 2014a). In the TEM micrograph (right) the structure of this kind of MWCNTs sample is shown. MWCNTs present a bamboo-like structure (Krueger, 2010) with a diameter between 15

and 30 nm. At the ends of the MWCNTs some nickel nanoparticles (the catalyst used for MWCNTs growth) may be observed.

For the characterization of the metal nanoparticles, we used XPS, ICP and TEM, once the nanoparticles were deposited on the MWCNTs in the device. The obtained results (metal loading, Cu/Pd molar ratio and nanoparticle size) are shown in Table 2.

Table 2| Nanoparticles deposited over the MWCNTs deposit characterization used in H_2 detection tests.

Sample	Nominal Metal Loading (% wt.)	Real Metal Loading (% wt.)[a]	Cu/Pd molar ratio[a]	Cu/Pd molar ratio[b]	Size ± σ (nm)[c]
0.3-Pd	0.3	0.29	-	-	2.4 ± 0.4
0.6-Pd	0.6	0.61	-	-	2.4 ± 0.4
1.2-Pd	1.2	1.19	-	-	2.4 ± 0.4
2.5-Pd	2.5	2.54	-	-	2.4 ± 0.4
1.2-$Cu_{0.25}Pd_{0.75}$	1.2	0.97	0.2/0.8 (0.25)	0.23/0.77 (0.29)	3,2 ± 0,8
1.2-$Cu_{0.5}Pd_{0.5}$	1.2	0.88	0.52/0.48 (1.10)	0.53/0.47 (1.12)	3,7 ± 1,0
1.2-$Cu_{0.75}Pd_{0.25}$	1.2	0.53	0.77/0.23 (3.35)	0.77/0.23 (3.35)	3,1 ± 0,8

[a] Metal loading and molar ratio determined by ICP-OES results.
[b] Molar ratio calculated by XPS results.
[c] Determined by TEM, diameter calculated after counting a minimum of 100 particles.

From Table 2, some important features are observed for pure Pd nanoparticles. In all samples prepared with the pure Pd nanoparticles the nominal metal loading is in excellent agreement with that obtained by ICP-OES. On the other hand, in Cu_xPd_{1-x} nanoparticles based devices, the real metal loading is in all cases lower than the nominal metal loading, and is strongly influenced by the Cu/Pd molar ratio in the synthesis procedure. We have observed that the real metal loading decreases with increasing Cu content in the deposited colloid. This evidences that not all the formed bimetallic nanoparticles were deposited over the MWCNTs during the synthesis and were either leached during the filtering step or were oxidized during handling of the sample. By means of ICP-OES and XPS results it is possible to obtain the Cu/Pd molar ratios between two different techniques which have a marked difference in terms of analysis depth. While in the former case the sample is dissolved (and thus bulk information on its composition is obtained), XPS can only analyze the outermost surface of the sample (the depth of analysis of the instrument used in this study is between 1 and 2 nm). Thus, the close similarity between the Cu/Pd ratios obtained both by ICP-OES and XPS indicates that the composition of the particles is identical both at the surface and in the bulk, which clearly indicates that the prepared CuPd nanoparticles form a solid solution, as expected from the Cu-Pd phase diagrams available in the literature (Baker and Okamoto, 2004). It must be noted that in all cases, the Cu/Pd molar ratios were very close to the target ratio in the synthesis.

The nanoparticles size observed by TEM once the nanoparticles are deposited over the MWCNTs before the H_2 detection tests, are very similar in all devices. The smaller nanoparticles are the pure Pd ones with an average diameter around 2.4 nm and a very narrow distribution. For Cu_xPd_{1-x} nanoparticles, the diameters obtained are somewhat larger than the pure Pd. However, in all cases the size of the CuPd nanoparticles is around

3.5 nm. The obtained sizes for all samples allow the direct comparison of all the prepared samples disregarding any possible size effect in the H_2 detection tests.

H_2 DETECTION TESTS

The results of the standard H_2 detection tests carried out in synthetic air for the Pd nanoparticles based devices are shown in Figure 3, in which the variation in resistance of the device is plotted versus time elapsed. In this figure, when the H_2 (3.3 % vol.) is introduced in the gas flow, the resistance of the samples changes. In all samples tested, a positive variation (resistance increase) during the H_2 pulse was registered. Pristine MWCNTs were tested in H_2 sensing devices without any resistance change, which evidenced the active role of the metal nanoparticle species.

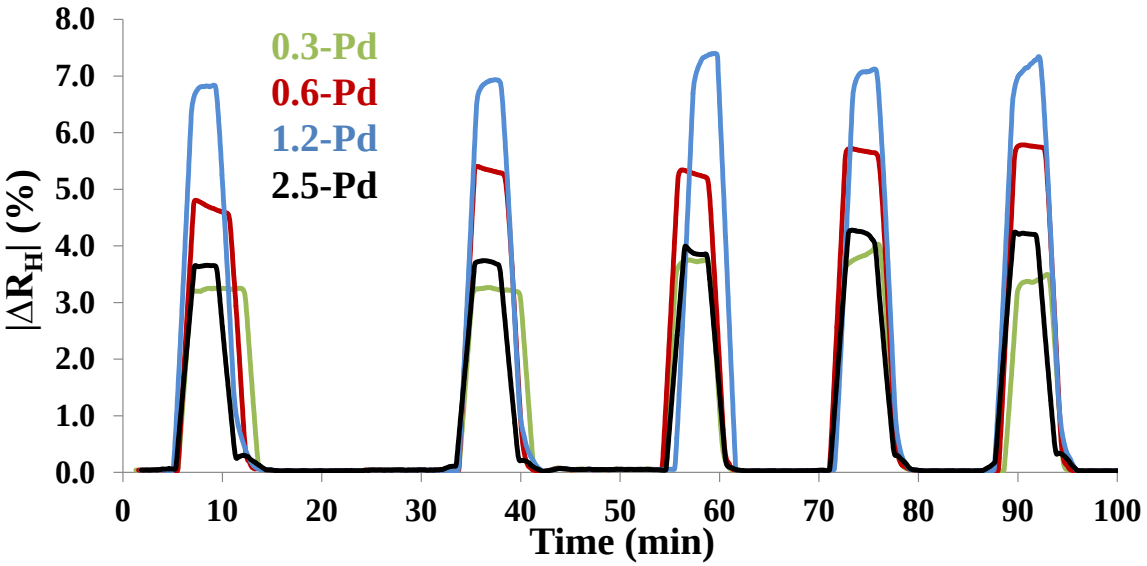

Figure 3. H_2 detection tests for devices coated with pure Pd nanoparticles with different metal loadings.

All the samples with Pd nanoparticles show very good activity in H_2 detection tests and a very reproducible signal is obtained during the passing of H_2-containing streams (3.3 % vol.) in synthetic air at room temperature. For the samples 0.3-Pd up to 1.2-Pd the obtained signal is proportional to the Pd metal loading. However, when the Pd loading increases up to 2.5 % wt. the sensitivity decreases to a value similar to that of the 0.6-Pd sample. This effect can also be seen in Figure 4, where the average values obtained for each sample versus the Pd loading are plotted. For this reason, we decided to analyze the samples after the H_2 detection tests by TEM. The most relevant results are shown in Figure 5.

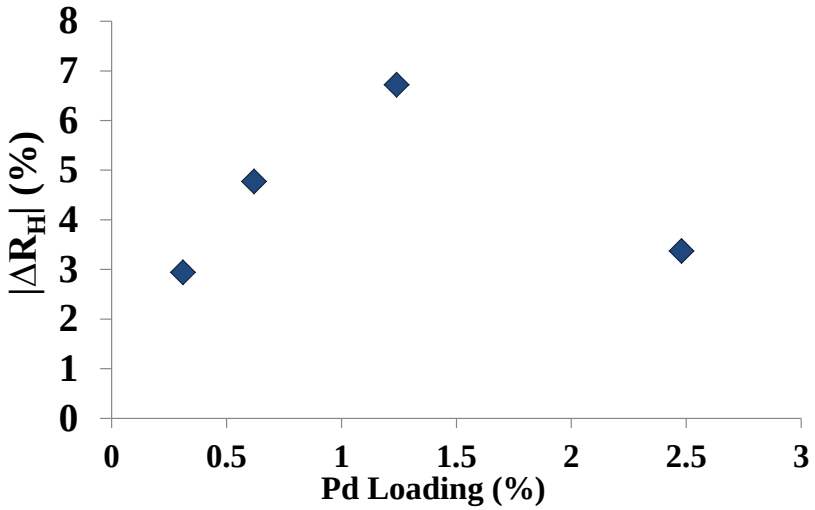

Figure 4| Average signal vs Pd metal loading of Pd-based MWCNTs devices in standard H_2 detection tests.

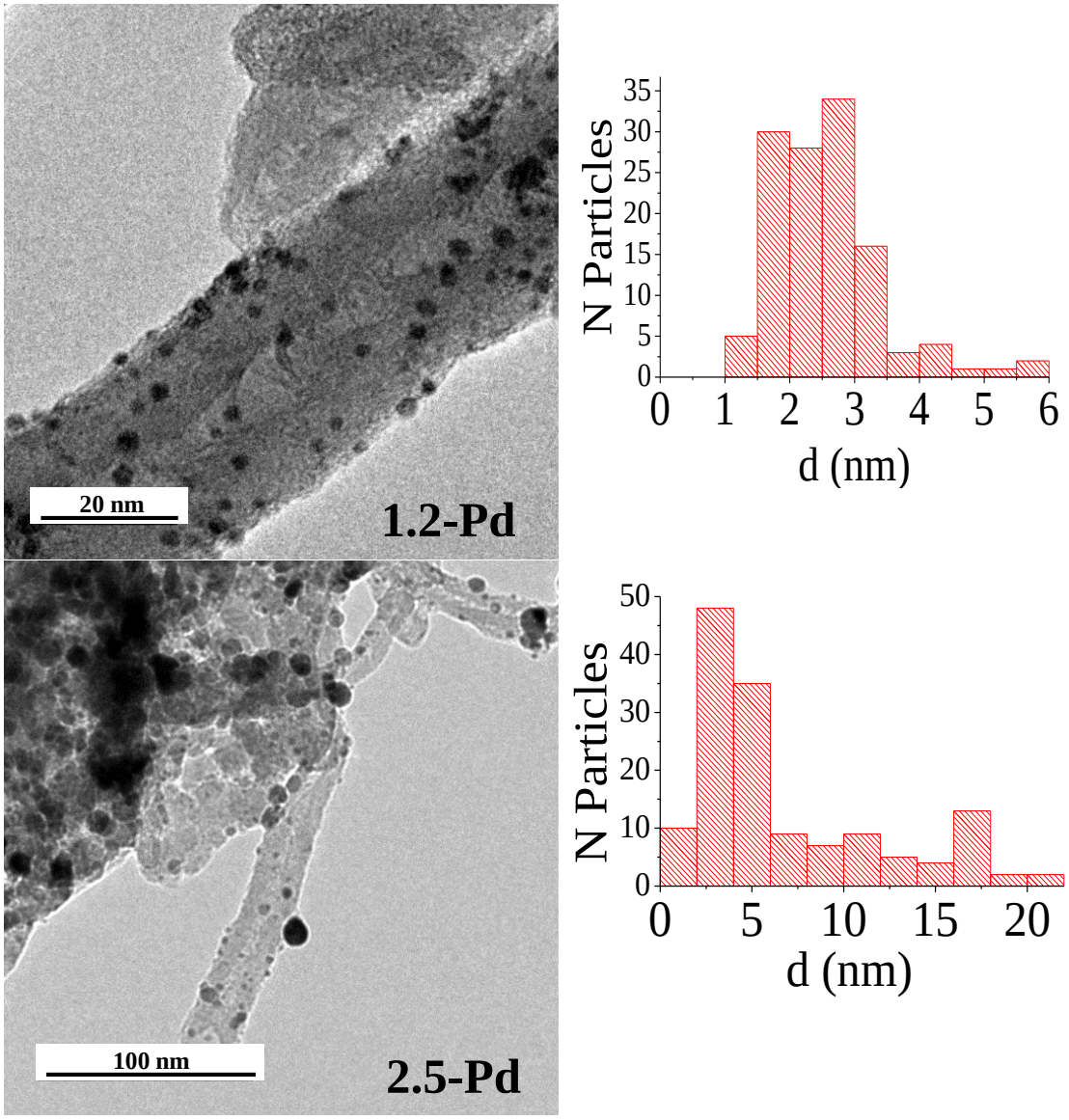

Figure 5| TEM pictures of 1.2-Pd (left) and 2.5-Pd (right) devices after the H_2 detection tests. A nanoparticles histogram of each sample is included to observe the final size of the Pd nanoparticles.

On one hand, for samples 0.3-Pd and 0.6-Pd (results not shown) no significant changes in the Pd nanoparticles size were observed by TEM. On the other hand, when the metal loading was increased to 1.2 % wt. (1.2-Pd sample) we could find some nanoparticles with a diameter around 5-6 nm as it can be seen in Figure 5 (left) which were possibly formed by the aggregation of several individual nanoparticles. In case of the sample with the

highest Pd loading (2.5-Pd) the histogram presented in Figure 5 (right) showed some nanoparticles larger than 20 nm. The increase of the nanoparticles size during the H_2 detection tests is due to the sintering between several neighboring nanoparticles. In this respect, the increase of metal loading entails the agglomeration of the nanoparticles on the external surface of the MWCNTs. When the devices were exposed to the H_2 (during the detection process) the nanoparticles sintered producing these large nanoparticles which impoverishes the performance of the sensors. For this reason, in sample 2.5-Pd a lower signal was obtained than the expected from its Pd metal loading.

In the light of these results, the Cu and Cu_xPd_{1-x} samples were prepared with a maximum nominal metal loading of 1.2% wt. with respect to the MWCNTs weight. The averaged results for each sample are shown in Figure 6. In this figure the H_2 sensing results normalized by the total metal loading and Pd ratio calculated by ICP-OES are also plotted in order to compare the samples and analyze the Pd effect and distribution.

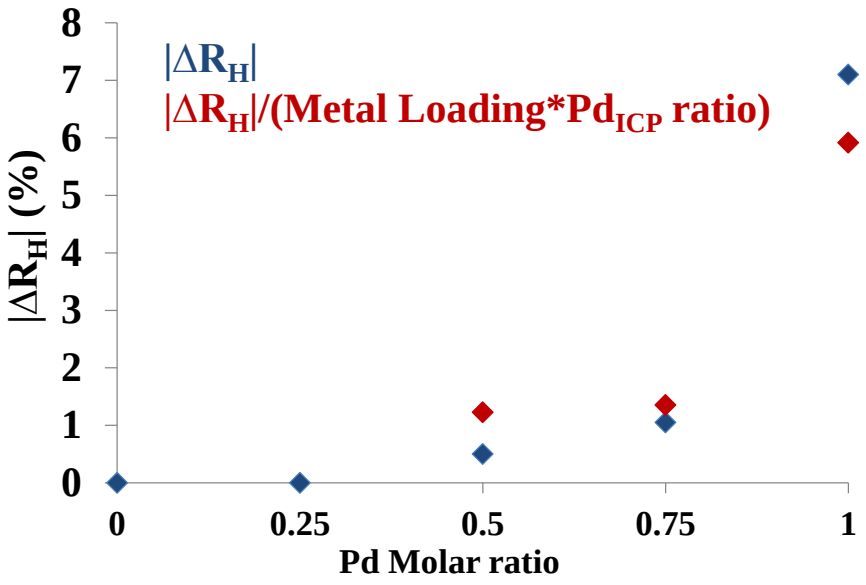

Figure 6| Average signal vs Pd molar ratio for the samples prepared with Cu_xPd_{1-x} nanoparticles in standard H_2 detection tests. Resistance variation obtained (blue) and resistance variation normalized with the ICP-OES metal loading and the ICP-OES Pd ratio (red).

In devices prepared with pure Cu and $Cu_{0.75}Pd_{0.25}$ nanoparticles no variation in the registered resistance was observed when the 3.3 % vol. of H_2 is introduced in the synthetic air gas flow. However, when the Pd fraction increases up to 50% (1.2-$Cu_{0.5}Pd_{0.5}$) a 1 % of resistance variation is obtained which increases up to 1.4 % in the sample 1.2-$Cu_{0.25}Pd_{0.75}$. These samples are very far from the device in which pure Pd nanoparticles with the same nominal metal loading were used. For this reason it became necessary to analyze the results normalizing the signal variation by the total metal amount, because in any Cu_xPd_{1-x}/MWCNTs the metal loading was very close to the nominal value. Since pure Cu nanoparticles seem irresponsive in the detection of H_2, it became also illustrative to divide the resistance increment by the Pd ratio (which was identified as the sole active species in the detection of H_2) calculated also by ICP-OES, as presented in Table 2. The calculated results are presented in Figure 6 (red dots). From these results the bimetallic samples 1.2-$Cu_{0.5}Pd_{0.5}$ and 1.2-$Cu_{0.25}Pd_{0.75}$ present a very similar sensing behavior, in good agreement with the ICP-OES and XPS results, where it was observed that the nanoparticles presented a homogeneous alloy between the two metals. However, they are not comparable with the pure Pd nanoparticles with the same nominal metal loading. Therefore, we may conclude that Cu does not improve on the properties of the Pd in the H_2 detection process.

Other experiments were performed to evaluate different properties of this kind of devices. Samples 0.6-Pd, 1.2-Pd and 1.2-$Cu_{0.25}Pd_{0.75}$ were selected to analyze the sensor response in streams with different H_2 concentrations (from 0.2 to 3.3 % vol.) in synthetic air. The results from this study are showed in Figure 7.

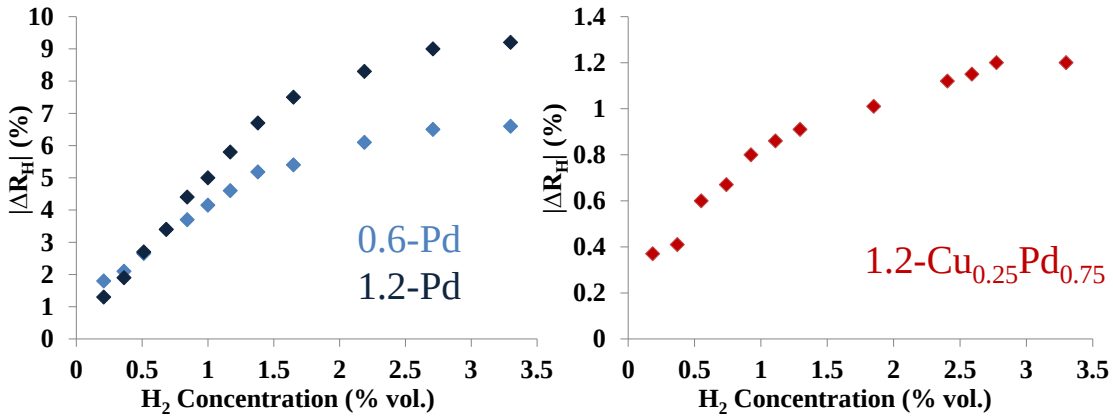

Figure 7| H_2 sensing signals for the different H_2 concentrations (% vol.) tested in this work. 0.6-Pd and 1.2-Pd (left) and 1.2-$Cu_{0.25}Pd_{0.75}$ (right).

The samples prepared in this study present a very good performance in the studied H_2 concentration range. The devices prepared with Pd nanoparticles have showed consistent and reproducible results. For lower H_2 concentrations (up to 1.5 % vol.) a linear correlation between the registered signal and the H_2 concentration in the stream is obtained. However, when the analyte concentration is above 2 % vol. the sensor response becomes saturated. Analyzing each sensor response for each H_2 concentration, as described in experimental section, it is possible to evaluate different parameters (response and recovery time) of the sensors to check their performance. For samples 0.6-Pd and 1.2-Pd, the response time is around 3 s for H_2 concentrations lower than 1 % vol. and 6 s for higher concentrations. The recovery time for each sample is in all cases lower than 60 s in all the studied H_2 concentration range.

In the sample with the bimetallic nanoparticles (1.2-$Cu_{0.25}Pd_{0.75}$) Figure 7 (right), less sensitivity is obtained in all the H_2 concentration range as in H_2 tests using synthetic air as carrier gas (Figure 6) while the observed response and recovery times were similar to those observed for the pure Pd sample. In this device, a different behavior than Pd-based

was obtained. The linear fit between signal and H_2 concentration was obtained for H_2 concentrations between 0.92 and 2.7 % vol.

DETECTION MECHANISM

In order to understand the H_2 detection process using nanoparticle-loaded MWCNTs, H_2 detection tests were carried out replacing the synthetic air for nitrogen as carrier gas while maintaining the H_2 concentration (3.3 % vol.). Both results for sample 1.2-$Cu_{0.25}Pd_{0.75}$ are shown in Figure 8, as an example of the results found for these MWCNT-based samples. After the last H_2 sensing pulse, pure synthetic air was introduced in both experiments to compare the results. It must be highlighted that all the devices prepared with MWCNTs and tested in this work have presented a positive increase of the resistance measured when H_2 was introduced in the gas stream. So, this resistance increase is attributed to a conductivity decrease in the device. In a previous study in our research group (García-Aguilar et al., 2014a), which devices were based on Pd nanoparticles (2-3 nm) loaded over SWCNTs (1-2 nm diameter), the resistance change was, in all cases, negative, as result of the conductivity increase.

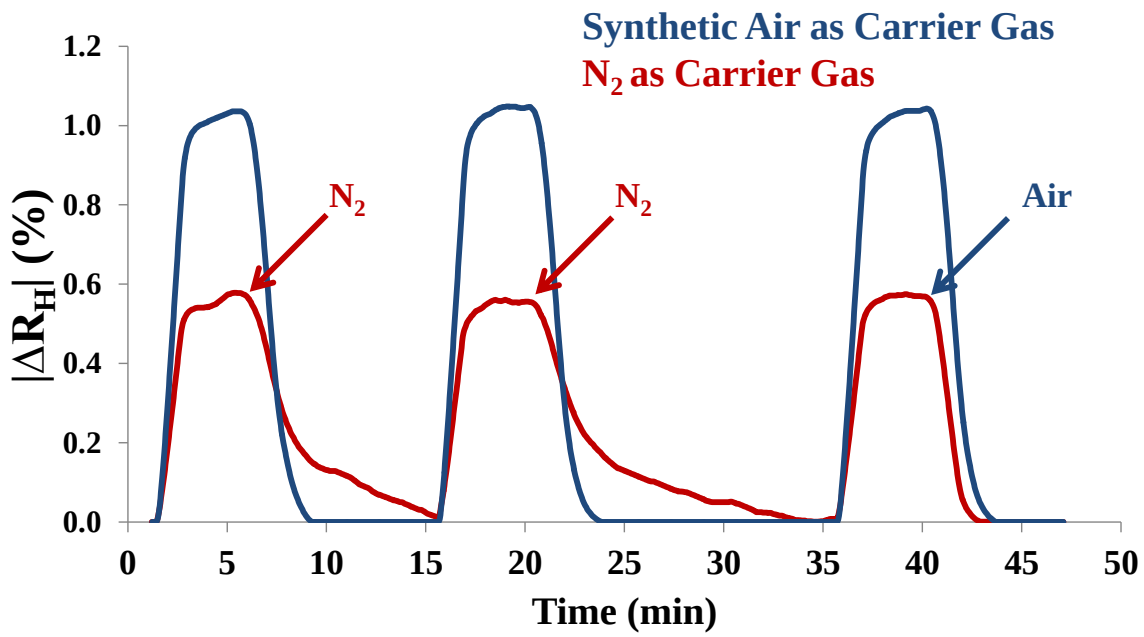

Figure 8| Standard H_2 test (blue) and H_2 test using N_2 as carrier gas (red) comparison for the sample $Cu_{0.25}$-$Pd_{0.75}$.

As shown in Figure 8, the presence of nitrogen (red line) in the device impoverishes the obtained signal (from 1 % to 0.5 % of resistance variation) and the recovery time (from few seconds to more than 10 minutes) of the sensor. The recovery of the device after passing H_2 over it when the gas stream is oxygen-depleted is very different compared with the results in synthetic air. In the former case, the recovery is significantly slower (around 10 minutes). However, when dioxygen is in the gas stream (recovery after the 3rd pulse in Figure 8), the recovery time decreases (down to 60 s). This change in the recovery mechanism is due to water formation. When H_2 is removed from the stream and the gas flow is switched to pure N_2, the recovery becomes slower because it will be determined by the desorption of hydrogen from the Pd nanoparticles. However, when O_2 is present the gas stream water is formed after the pulse, allowing the fast recovery of the device. Nevertheless, the signal recovers completely what is an important difference compared to the previous study done with the SWCNT in which the recovery was absent unless air was

used. It must be said that although this recovery is slower in oxygen-depleted atmospheres for MWCNT, it represents a clear and distinct improvement from our previous results using Pd-based nanoparticles supported on SWCNTs (García-Aguilar et al., 2014a) in which oxygen was indispensable for the recovery of the sensors. In this sense, the use of an oxygen-depleted atmosphere rendered the device insensitive after three H_2 pulses due to saturation of the device. These differences in the recovery in N_2 atmosphere is a consequence of the predominant detection mechanism in each case.

There are two main detection mechanisms reported for these kinds of sensors based on carbon nanomaterials, one produced by the Pd nanoparticles increasing their size due to hydrogen absorption (up to 15%), in which conductivity increases and resistance decreases due to the growth of the Pd particles establishing new connections through which electrons may travel (Favier et al., 2001). On the other hand, when the Pd nanoparticles absorb H_2, the Pd hydride is formed, which is known to have a lower work function than pure Pd, so transfer of electrons to the nanotubes may occur. This, in turn, would reflect as an increase in the resistance of the system provided that the CNTs are p-type semiconductor. In this latter example, conductivity decreases and resistance increases (Lim et al., 2013, Randeniya et al., 2012) Consequently, the observed behaviour of the sensors is the result of the two competitive mechanisms taking place at the same time on the sample. In the case of Pd-SWCNTs samples, the predominant mechanism is the first one and the main recovery mechanism that produces the return to the initial resistance value is the decrease in the Pd nanoparticles size due to water formation in the presence of oxygen (García-Aguilar et al., 2014a; Lin and Huang, 2012).

However, for the Pd containing MWCNTs used in this work, the predominant mechanism is the increase in resistance due to electron transfer from the Pd nanoparticles to the CNT, coming these electrons from the reaction between hydrogen and Pd. In this case, the

change in size of Pd nanoparticles upon hydrogen absorption does not have a significant contribution considering that the different size between the nanoparticles (2-3 nm) and the MWCNTs (15-30 nm) reduces the effect of this phenomenon more than in the case of SWCNTs, in which both materials had approximately the same diameter (García-Aguilar et al., 2014a). The recovery of the signal in N_2 is mainly due to the decrease in electron density at the interface between the Pd nanoparticles and the MWCNT as a consequence of hydrogen desorption. It seems that significant changes in electron density occurs at the interface in N_2 atmosphere although slower than in air, thus observing a recovery of the signal after longer times.

DISCUSSION

This work combines the preparation of polymer-protected metal nanoparticles synthesized by a well-established methodology with the use of carbon nanomaterials for the development of composites which show a good behaviour in H_2 sensing applications. The prepared nanoparticles have proven to be stable under operation, although at high metal loadings the formation of larger metallic aggregates is also observed. It must be noted that the inclusion of Cu in the formed nanoparticles brings about two main differences: (1) the formation of a Cu-Pd alloy phase (as confirmed by ICP-OES and XPS) and (2) a significant reduction in the cost of preparation of the nanoparticles due to the lower price of Cu(II) precursors as compared to Pd(II) precursors. The devices prepared from these alloy phase, however perform poorly compared to pure Pd nanoparticles, indicating the inability of Cu to interact with gaseous H_2 in a manner that would allow its detection in this type of sensors based on resistivity variations. This has been evidenced when the results on resistivity changes are normalized per mol of metallic Pd (Figure 6) in which the

presence of Cu must be seen as largely detrimental. Thus, our study has revealed that sample 1.2-Pd deposited on MWCNTs has yielded the device which presents the best sensing properties (sensibility, response and recovery time and accuracy in H_2 detection). These devices must be compared with the same kind of carbon nanomaterials (SWCNTs and MWCNTs). Some works based on these kinds of materials have presented better sensing results than the materials reported in this study. However, it must be said that in these cases, the preparation methodology to incorporate the metal on the carbon material is more elaborate (Ju et al., 2010; Lin and Huang, 2012; Rumiche et al., 2012). There are also some works based on MWCNTs doped with Pt by chemical vapor deposition (Kumar and Ramaprabhu, 2006) with sensibility results similar to those reported in this work. In this context, one previous work in our research group (García-Aguilar et al., 2014a) used relatively large amounts of mixed surfactants (sodium dodecylbenzenesulfonate and PVP) as dispersing agent in aqueous suspensions of SWCNTs with devices showing better sensing results. On the other hand, the presented results show a better sensing performance than other works found in the literature using Pd-based devices, prepared either by sputtering or Pd-Pt by electrochemical method, on CNTs (Ding et al., 2007; Randeniya et al., 2012), respectively.

To sum up, in this work we have presented a very simple and cost-efficiency methodology to prepare H_2 sensing devices with very interesting results using MWCNTs without any purification treatment and avoiding the use of surfactants in their suspension. The influence of Pd metal loading or the inclusion of alloyed Cu in the nanoparticles composition has been analyzed. In the most promising devices the effect of H_2 concentration in the gas stream and working in oxygen-depleted atmospheres have been analyzed to understand the samples performance. The study of these samples prepared with MWCNTs allows the comparison of different detection mechanisms (compared with

our previous work using SWCNTs) with the modification of the carbon nanomaterial. These devices are perfectly comparable with other results found in the literature and very promising for H_2 detection at ambient conditions (room temperature and pressure).

ACKNOWLEDGMENTS

We thank the MINECO, GV and FEDER (Projects CTQ2012-31762 and PROMETEOII/2014/010) for financial support. J.G.A. thanks the Spanish Ministry of Economy and Competitiveness (MINECO) for his fellowship (BES-2013-063678).

REFERENCES

Abbasi, T., and Abbasi, S. A. (2011). "Renewable" hydrogen: Prospects and challenges. *Renew. Sustain. Energy Rev.* 15, 3034–3040. doi:10.1016/j.rser.2011.02.026.

Baker, H., and Okamoto, H. (2004). *ASM handbook, volume 3 - Alloy Phase Diagrams*.

Boon-Brett, L., Black, G., Moretto, P., and Bousek, J. (2010). A comparison of test methods for the measurement of hydrogen sensor response and recovery times. *Int. J. Hydrogen Energy* 35, 7652–7663. doi:10.1016/j.ijhydene.2010.04.139.

Ding, D., Chen, Z., Rajaputra, S., and Singh, V. (2007). Hydrogen sensors based on aligned carbon nanotubes in an anodic aluminum oxide template with palladium as a top electrode. *Sensors Actuators, B Chem.* 124, 12–17. doi:10.1016/j.snb.2006.11.034.

Domínguez-Domínguez, S., Berenguer-Murcia, Á., Cazorla-Amorós, D., and Linares-Solano, Á. (2006). Semihydrogenation of phenylacetylene catalyzed by metallic nanoparticles containing noble metals. *J. Catal.* 243, 74–81. doi:10.1016/j.jcat.2006.06.027.

Du, Y., Xue, Q., Zhang, Z., and Xia, F. (2014). Great enhancement in H_2 response using graphene-based Schottky junction. *Mater. Lett.* 135, 151–153. doi:10.1016/j.matlet.2014.07.141.

Favier, F., Walter, E. C., Zach, M. P., Benter, T., and Penner, R. M. (2001). Hydrogen sensors and switches from electrodeposited palladium mesowire arrays. *Science* 293, 2227–2231. doi:10.1126/science.1063189.

García-Aguilar, J., Miguel-García, I., Berenguer-Murcia, Á., and Cazorla-Amorós, D. (2014a). Single wall carbon nanotubes loaded with Pd and NiPd nanoparticles for H_2 sensing at room temperature. *Carbon* 66, 599–611. doi:10.1016/j.carbon.2013.09.047.

García-Aguilar, J., Miguel-García, I., Berenguer-Murcia, A., and Cazorla-Amorós, D.

(2014b). Synthesis of Robust Hierarchical Silica Monoliths by Surface- Mediated Solution/Precipitation Reactions over Different Scales: Designing Capillary Microreactors for Environmental Applications. *ACS Appl. Mater. Interfaces* 6, 22506–22518.

Goldoni, A., Petaccia, L., Lizzit, S., and Larciprete, R. (2010). Sensing gases with carbon nanotubes: a review of the actual situation. *J. Phys. Condens. Matter* 22, 013001. doi:10.1088/0953-8984/22/1/013001.

Hübert, T., Boon-Brett, L., Black, G., and Banach, U. (2011). Hydrogen sensors – A review. *Sensors Actuators B Chem.* 157, 329–352. doi:10.1016/j.snb.2011.04.070.

Ju, S., Lee, J. M., Jung, Y., Lee, E., Lee, W., and Kim, S. J. (2010). Highly sensitive hydrogen gas sensors using single-walled carbon nanotubes grafted with Pd nanoparticles. *Sensors Actuators, B Chem.* 146, 122–128. doi:10.1016/j.snb.2010.01.055.

Kaniyoor, A., and Ramaprabhu, S. (2011). Hybrid carbon nanostructured ensembles as chemiresistive hydrogen gas sensors. *Carbon* 49, 227–236. doi:10.1016/j.carbon.2010.09.008.

Krueger, A. (2010). *Carbon Materials and nanotechnology,* 163. Wiley-VCH doi:10.1002/9783527629602.

Kumar, M. K., and Ramaprabhu, S. (2006). Nanostructured Pt functionlized multiwalled carbon nanotube based hydrogen sensor. *J. Phys. Chem. B* 110, 11291–8. doi:10.1021/jp0611525.

Lim, J., Hwang, S., Yoon, H. S., Lee, E., Lee, W., and Jun, S. C. (2013). Asymmetric electron hole distribution in single-layer graphene for use in hydrogen gas detection. *Carbon* 63, 3–8. doi:10.1016/j.carbon.2013.05.071.

Lin, T. C., and Huang, B. R. (2012). Palladium nanoparticles modified carbon nanotube/nickel composite rods (Pd/CNT/Ni) for hydrogen sensing. *Sensors Actuators B Chem.* 162, 108–113. doi:10.1016/j.snb.2011.12.044.

Miguel-García, I., Navlani-García, M., García-Aguilar, J., Berenguer-Murcia, Á., Lozano-Castelló, D., and Cazorla-Amorós, D. (2015). Capillary microreactors based on hierarchical SiO_2 monoliths incorporating noble metal nanoparticles for the Preferential Oxidation of CO. *Chem. Eng. J.* 275, 71–78. doi:10.1016/j.cej.2015.04.020.

Phan, D. T., and Chung, G. S. (2014). Reliability of hydrogen sensing based on bimetallic Ni–Pd/graphene composites. *Int. J. Hydrogen Energy* 39, 20294–20304. doi:10.1016/j.ijhydene.2014.10.006.

Randeniya, L. K., Martin, P. J., and Bendavid, A. (2012). Detection of hydrogen using multi-walled carbon-nanotube yarns coated with nanocrystalline Pd and Pd/Pt layered structures. *Carbon* 50, 1786–1792. doi:10.1016/j.carbon.2011.12.026.

Rumiche, F., Wang, H. H., and Indacochea, J. E. (2012). Development of a fast-response/high-sensitivity double wall carbon nanotube nanostructured hydrogen sensor. *Sensors Actuators, B Chem.* 163, 97–106. doi:10.1016/j.snb.2012.01.015.

Shenderova, O. A., Zhirnov, V. V., and Brenner, D. W. (2002). Carbon Nanostructures. *Crit. Rev. Solid State Mater. Sci.* 27, 227–356. doi:10.1080/10408430208500497.

Wang, Z., Liu, S., Jiang, T., Xu, X., Zhang, J., An, C., et al. (2015). N-type SnO_2 nanosheets standing on p-type carbon nanofibers: a novel hierarchical nanostructures based hydrogen sensor. *RSC Adv.* 5, 64582–64587. doi:10.1039/C5RA08863A.

Zaragoza-Martín, F., Sopeña-Escario, D., Morallón, E., and de Lecea, C. S. M. (2007). Pt/carbon nanofibers electrocatalysts for fuel cells. Effect of the support oxidizing treatment. *J. Power Sources* 171, 302–309. doi:10.1016/j.jpowsour.2007.06.078.